

# EVALUATION OF THE STRUCTURE, MICROHARDNESS AND CORROSION PROPERTIES OF COBALT-CHROMIUM DENTAL ALLOYS WITH TWO DIFFERENT COOLING MEDIA

**Cristina Jiménez-Marcos** 

Mechanical Engineering Department, Las Palmas de Gran Canaria University, 35014 Las Palmas de Gran Canaria, Spain

**Julia Claudia Mirza-Rosca** 

Mechanical Engineering Department, Las Palmas de Gran Canaria University, 35014 Las Palmas de Gran Canaria, Spain  
Materials Engineering and Welding Department, Transilvania University of Brasov, 500036 Brasov, Romania

**Dinu Vermesan** 

Department XV, Orthopedics – Traumatology, Urology and Medical Imaging “Victor Babeş” University of Medicine and Pharmacy in Timișoara, 300041 Timișoara, Romania

**Adriana Saceleanu** 

Faculty of Medicine, Lucian Blaga University of Sibiu, 550024 Sibiu, Romania

Copyright © 2025 The Author(s)  
<https://doi.org/10.1007/s40962-025-01596-6>

## Abstract

*This study investigates the impact of cooling rate after heat treatment on the electrochemical and microstructural properties of three dental Co-Cr alloys. Advanced techniques, such as scanning electron spectroscopy and X-ray diffraction, were used to evaluate the microstructures and compositions of the alloys, revealing the influence of elements such as tungsten and niobium on their electrochemical behavior. The results have shown that the alloys with 5%Mo exhibited higher porosity than the alloy with Nb and W. High melting temperature due to the presence of Nb and W ensured a more homogeneous material and a slightly altered structure. For all alloys, heat-treated samples showed higher microhardness compared with*

*casting samples. A passive behavior was observed for all the samples with the best stability at high potential for the alloy with the highest Cr content due to the formation of a protective Cr<sub>2</sub>O<sub>3</sub> passive layer. Water-quenched samples showed high impedance values, demonstrating their effectiveness in corrosion resistance. The choice of cooling methods and alloy composition is crucial for improving corrosion resistance and mechanical properties of dental frameworks.*

**Keywords:** Co-Cr alloys, heat treatment, microstructure, corrosion, microhardness

## Introduction

The use of dental prostheses with metallic structures has its roots in ancient civilizations, such as the Egyptians, Greeks, and Romans, where metals like gold and silver were used

to create dental restorations. In the 18th century, more advanced techniques were introduced, such as the use of gold wires to anchor artificial teeth to adjacent natural teeth, resulting the first version of today's dental bridges.<sup>1</sup>

However, at the beginning of the 20th century, dental laboratories began to develop veneering ceramics deposited on metallic framework materials, based on chromium, specifically designed for use in dentistry, with the nickel-chromium (Ni-Cr) and cobalt-chromium (CO-CR) alloys standing out. These alloys were and are still used to create

---

This paper is an invited submission to IJMC selected from presentations at the 3rd Carl R. Loper Conference on Processing of Metallic Materials through Casting and Solidification held September 23-25, 2024, at the Sergiu T. Chiriacescu Aula of Transilvania University, Brasov, Romania.

Received: 05 December 2024 / Accepted: 26 February 2025  
Published online: 21 April 2025

more durable and complex prostheses, such as crowns, bridges and removable partial dentures.<sup>2,3</sup>

Ni-Cr alloys are known for their excellent corrosion resistance, low thermal expansion and high mechanical strength, which makes them especially useful for dental restorations in posterior teeth, where masticatory forces are more intense.<sup>4-7</sup> However, despite these advantages, Ni-Cr alloys have several drawbacks that have raised concerns in the medical community and have encouraged the search for safer alternatives.

One of the main problems with Ni-Cr alloys is the release of metal ions during prolonged exposure to oral fluids. These ions, particularly nickel ions, can trigger adverse immunological responses, including allergic reactions in a significant percentage of the population. It is estimated that a 14.5% of European people are sensitive to nickel, which can lead to contact dermatitis, hypersensitivity and even more severe systemic reactions.<sup>8</sup> In addition, nickel has been classified as a probable carcinogen by International Agency for Research on Cancer (IARC, part of the World Health Organization, Group 1), which has raised concerns about its use in long-term medical applications.<sup>4,9,10</sup>

For these reasons, there has been a growing trend to opt for Co-Cr alloys instead of Ni-Cr alloys, particularly in patients with a history of metal sensitivity or allergy. Co-Cr alloys have a number of advantages that have made them a preferred alternative in many countries.<sup>11,12</sup> Cobalt-based alloys are characterized by their high wear, resistance to creep, corrosion, temperature, hardness and magnetism.<sup>3,12-14</sup> In addition, dental materials made from such alloys can perform their functions without compromising the patient due to their proven cytocompatibility.<sup>12,15</sup> These alloys offer high corrosion resistance because of the of a passive chromium oxide ( $\text{Cr}_2\text{O}_3$ ) layer on the surface, which prevents the release of metal ions into the oral cavity and minimizes the risk of adverse reactions.<sup>16-18</sup> By creating a protective surface oxide coating, Cr, which is added at a rate of 11-33%, improves the alloy's chemical stability, increases the alloy's resistance to oxidation at high temperatures and prevents corrosion.<sup>11,19,20</sup>

Despite the extremely low number of people experiencing allergic responses due to the use of cobalt-chromium alloys, the body may nevertheless experience certain side effects from the discharge of metal ions from the alloy. In addition, cobalt was added to the list of carcinogenic, mutagenic and toxic to reproduction (CMR) compounds in 2020, indicating the need for further studies on its possible long-term effects.<sup>14,21,22</sup>

Modern Co-Cr alloys include alloying elements that improve their performance in the oral environment. Molybdenum (Mo) increases the density, hardness and compressive strength of the alloy without affecting its

ductility, which is crucial in dental frameworks exposed to wet and tensile conditions.<sup>18,23,24</sup> Niobium (Nb) acts as a grain refiner, increasing the strength as well as the elongation, making it suitable for patients with hypersensitivity to other metals.<sup>24-26</sup> Finally, tungsten (W) stabilizes the co-matrix structure, improving the passivity and resistance to pitting corrosion.<sup>23</sup> Together, these elements give to Co-Cr alloys exceptional mechanical strength, thermal stability and durability in the oral cavity.

In addition to alloy composition, the heat treatment and specially the cooling rate play a main role in the final microstructure and mechanical properties of dental prostheses. Rapid water quenching and slow furnace cooling have notable effects on phase formation within the alloy. Quenching can generate internal stresses and the formation of harder phases, such as martensite, which, while increasing hardness, can make the alloy more susceptible to intergranular corrosion. On the other hand, furnace cooling favors stress relaxation and homogenization of the alloying elements, although it is sometimes associated with a growth in grain size, which can compromise mechanical strength.<sup>27-29</sup>

The present study focuses on the analysis of three commercial Co-Cr alloys with additions of Mo, Nb, W and Si (silicon) for the frameworks. It is investigated how the cooling methods, such as furnace slow cooling and water quenching, influence their electrochemical and mechanical properties, especially corrosion resistance and hardness. Techniques such as metallography, X-ray diffraction, scanning electron microscopy, electrochemical and microhardness testing are used by comparing three dental alloys with different compositions and cooling rates. This approach seeks to identify optimal configurations for use in the manufacture of dental crowns and bridges, where biocompatibility and durability are essential.

## Experimental

### Samples Preparation

As a preliminary step to microstructural analysis, electrochemical and microhardness testing, several pre-processing steps were carried out by cutting the alloys (namely S1, S2 and S3) ingots into circular disks with a Buehler IsoMet 4000 precision saw (Chicago, Illinois, USA). Two samples from each alloy were exposed to heat treatment for one hour at 900°C in a Heron model 12 PR/300 BB series muffle furnace with the nominal voltage of 220V and the temperature stability of  $\pm 3^\circ\text{C}$ . The heat treatment process was performed at a heating rate of 25°C/min and after, the cooling method was different: (i) a sample of each alloy was cooled in water named SW and (ii) a sample of each alloy was left in the heat treatment oven and cooled with the oven off for 24 hours, named SOv.

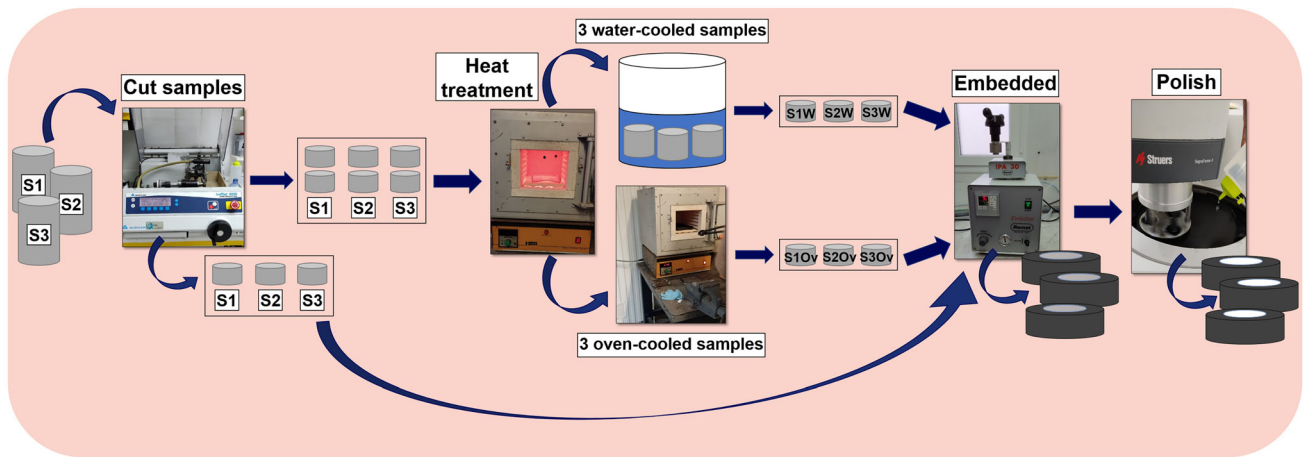


**Figure 1. Studied alloys preparation.**

**Table 1. Composition (in wt%) of the Alloys Under Study According to the Manufacturer**

Sample	Composition (wt%)									
	Co	Cr	Mo	W	Nb	C	Fe	Si	Mn	
S1	61.00	31.00	5.00	–	–	0.75	0.75	0.75	0.75	
S2	63.00	28.00	0.50	4.00	3.00	1.00	–	–	0.50	
S3	64.00	28.50	5.00	–	–	1.00	1.00	0.50	–	

The samples were hot mounted by using phenolic resin in a hot mounting press (Remet filler model IPA 30 Evolution) at 170°C. Afterward, the samples were prepared by grinding and polishing using the Struers TegraPol-11 polisher (Copenhagen, Denmark), using 400 to 2500 grit progressive silicon carbide abrasive papers and, finally, 0.1 micrometer alpha-alumina suspension polishing cloths to achieve a final mirror polish.<sup>30</sup> The metallography samples were prepared following the guidelines of ASTM E3-11(2017)<sup>31</sup> (see Figure 1).

Table 1 shows the chemical composition of the commercial alloys used in the present study:

### Phase Analysis

For phase analysis, an Empyrean Malvern-Panalytical diffractometer (Malvern, UK) was utilized for samples S1, S2 and S3. For the research, a CuK radiation (1.5406 Å) with a step size of 0.02°, a current of 40 mA and a power of 45 kV was utilized in the range of  $2\theta = 10 - 80$ .

### Microstructural Analysis

For metallographic analysis, a metallographic microscope (Olympus BX-51, Tokyo, Japan) was used. Prior to the investigation, the study samples were immersed in an Aqua Regia reagent, which consists of 15 mL HCl, and 5 mL HNO<sub>3</sub>, for around 60–120 s. A scanning electron microscope (Zeiss Sigma 300 VP, Carl Zeiss, Jena, Germany) combined with an energy-dispersive X-ray spectrometer (EDX) was used for microstructural and elemental analysis.

### Microhardness Test

The Vickers hardness test was employed in order to evaluate the microhardness of the alloys before and after heat treatment. Ten measurements were taken with the Future Tech FM-810 hardness tester in compliance with ISO 14577-1:2015.<sup>32</sup> For the measurements, a load of 10 gf and a holding time of 15 seconds were utilized.

## Electrochemical Tests

According to ISO 10271:2020,<sup>33</sup> three electrodes were employed for the electrochemical tests: a working electrode (the sample under examination), a reference electrode (saturated calomel) and a counter electrode (platinum electrode). The area of each sample under study was determined in order to conduct the experiments. The following components, measured in mmol/L, compose the Ringer Grifols solution (Grifols Laboratories, Barcelona, Spain):  $\text{Na}^+$  129.90;  $\text{K}^+$  5.40;  $\text{Cl}^-$  111.70;  $\text{C}_3\text{H}_5\text{O}_3$  27.20 and  $\text{Ca}^{2+}$  1.80. The corrosion behavior of the alloys was investigated employing a potentiostat-galvanostat BioLogic Essential SP-150 (Seyssinet-Pariset, France) with the techniques: open-circuit potential, linear polarization and electrochemical impedance spectroscopy are the three methods used.

Each sample's 24-h open-circuit potential was determined using the " $E_{\text{corr}}$  versus Time" method found in the EC-Lab program. To obtain the corrosion rate, "Linear Polarization" was applied with a potential scanning rate of 10.00 mV/minute in the range from  $-0.70$  V to  $1.00$  V vs. SCE. For the impedance measurements, "Potentiometric Electrochemical Impedance Spectroscopy" was selected following ISO 16773-1:2016.<sup>34</sup> The scanning frequency of 100 KHz to 100 MHz was applied, and Nyquist and Bode diagrams were used to plot the obtained data. Furthermore, an electrical equivalent circuit was used to fit the experimental data.

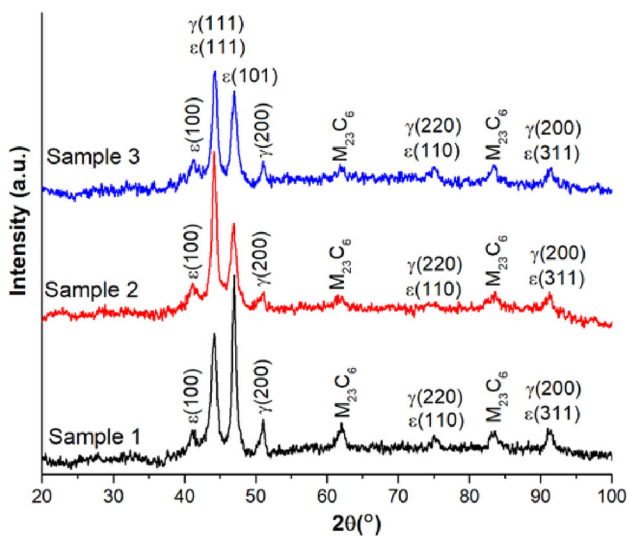


**Figure 2.** XRD spectra for the three samples: S1 (a), S2 (b) and S3 (c).

## Results and Discussion

### Phase Analysis

The studied alloys' XRD spectra are displayed in Figure 2. The primary phases of the samples were determined by the analysis to be  $\epsilon$  with a hexagonal close-packed structure (HCP) and  $\gamma$  with a body-centered cubic structure (FCC), along with minor phases of different metallic carbides. Sample S1 exhibited predominant levels of HCP  $\epsilon$ -phase, whereas FCC  $\gamma$ -phase predominates in samples S2 and S3.

### Microstructural Analysis

Figure 3 shows images of the surfaces of the three samples after etching that were left untreated (S1, S2 and S3), three that were heat-treated and quenched in water (S1W, S2W and S3W), and three that were heat-treated and cooled in the oven for 24 h (S1Ov, S2Ov and S3Ov). The microstructure of the examined samples was dendritic, which is common for cast materials. The samples are characterized by a chemically heterogeneous microstructure consisting of an austenitic matrix of cobalt-chromium solution in a core dendritic microstructure.

The dendritic structures of samples S1 and S3 are similar and slightly different for sample S2 because of the addition of niobium and tungsten. The structure of the heat-treated samples is similar to their corresponding untreated samples. However, some differences can be noted: the samples cooled in the oven show a coarsening of the dendrites, while those cooled in water show finer dendrites.

Figure 4 presents the samples microstructure prior to heat treatment investigated by using SEM and a BSD detector in order to reveal the different phases formed within the samples during casting. In accordance with the optical microscopy investigation, the SEM analysis revealed the dendritic structure with different phases at higher magnification. The interdendritic areas composed by M23C6 carbide type which was revealed by the XRD investigation are embedded in Co-rich solid solution dendrites. From the EDX spectra, it can be seen that the interdendritic structure presents an increased amount of alloying elements such as Mo or Nb embedded in a rich Co-Cr-rich matrix. In the case of sample S1 and S3, some dark areas might be noticed on the micrographs, which, in accordance with the EDX spectra, reveal locally the formation of Si-rich carbides. In sample S2, eutectic lamellar carbides (M23C6) might be noticed (labeled with 2 on the micrographs) embedded in the  $\gamma$  (FCC) Co-rich solid solution. In sample S1 and S3, some pores might be noticed formed during casting. The absence of pores in sample S2 can be explained by the presence of Nb and W in the composition with high melting points ( $2477^\circ\text{C}$  and  $3422^\circ\text{C}$ , respectively) and due to this the casting process is carried out at a

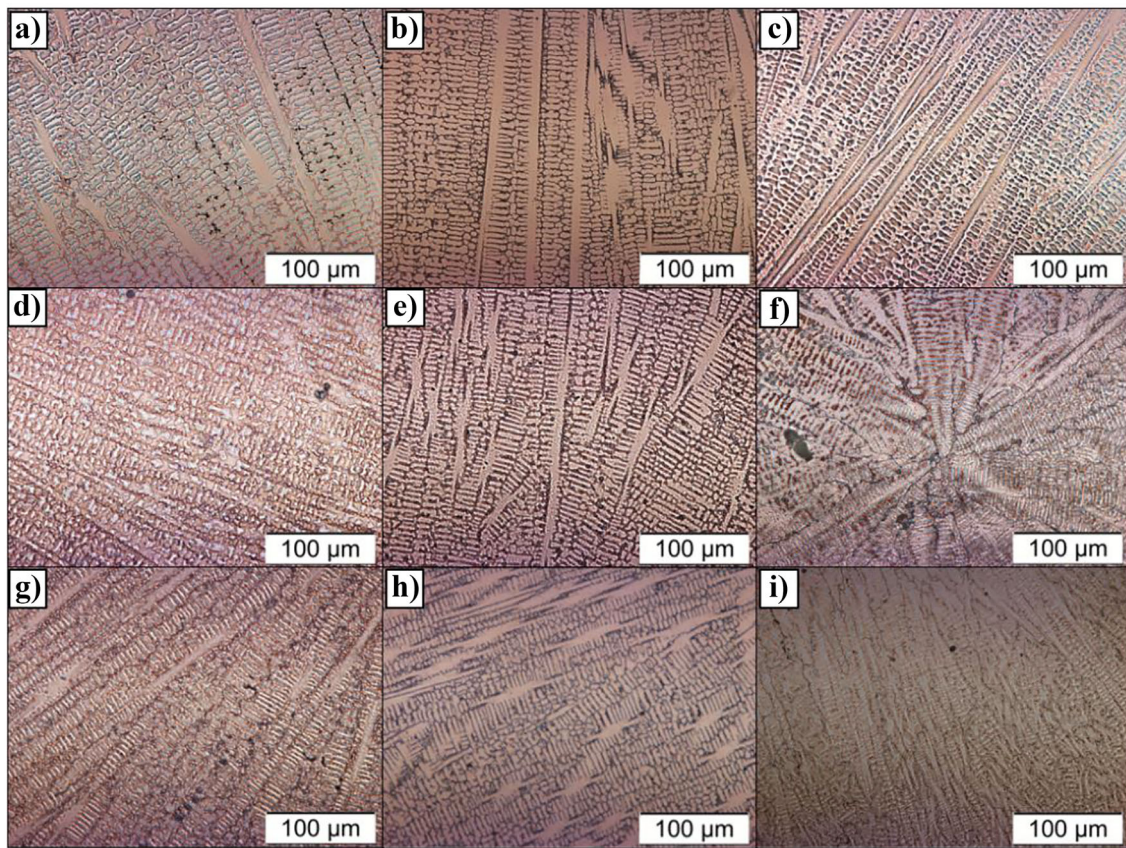


**Figure 3. Microstructure by optical microscopy of the S1 (a), S1W (b), S1Ov (c), S2 (d), S2W (e), S2Ov (f), S3 (g) S3W (h) and S3Ov (i) samples after chemical etching.**

higher temperature, which ensures a better homogeneity of the sample.

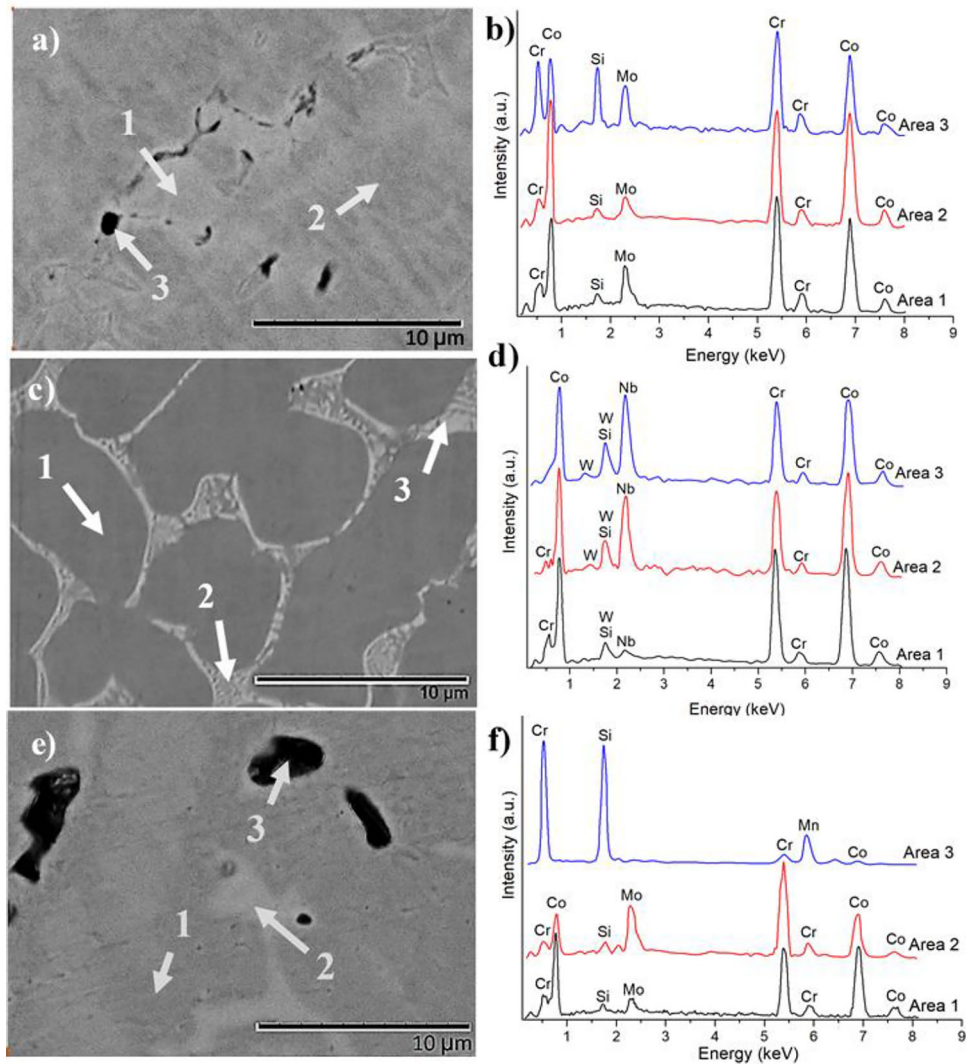
After heat treatment and cooling in the oven for 24 h, the microstructure is similar to commercial materials. The dendritic regions are rich in Co solid solution, while the interdendritic area is composed of Cr-rich regions (labeled with 2 for Sample S1Ov) and M23C6 carbides (labeled with 3 for sample S1Ov). However, a few differences can be noticed in Figure 5: In Samples S1Ov and S3Ov, the interdendritic regions are rich in Cr and carbides. Sample S2Ov shows reduced lamellar carbides in the interdendritic areas compared to the untreated sample.

Figure 6 shows the micrographs and EDX spectra of samples after heat treatment and water quenching. In general, the microstructure is similar to that of the oven-cooled samples. Some differences can be seen, such as the formation of lamellar carbides in sample S1W (labeled 2 in Figure 6a), the concentration of Cr in the interdendritic regions (labeled 3 in Figure 6a); the widening of the interdendritic regions and the formation of an increased number of lamellar carbides (labeled 2 in Figure 6c).

### Microhardness Test

Figure 7 and Table 2 show the microhardness values HV0.01, together with the average, the standard deviation, the maximum and minimum values and the depth of the indentation, obtained from the 10 indentations performed on each specimen. Applying 10 gf to each sample, the microhardness values vary over a wide domain, mainly for S1Ov, indicating scatter in the data. The maximum values of the samples vary between 310 and 380, while the minimum values appear between 200 and 290 HV. This fact may mean the presence of soft and hard areas on the surface of the specimens due to the manufacturing process of the samples. In general, an increase in hardness results and, therefore, a decrease in the depth of the footprint is observed for the samples that have been heat treated.

As was revealed by EDS and XRD analysis, the Cr-rich carbide is identified in the microstructure of the alloys, embedded in Co-rich solid solution. The hard phase is the Cr-carbide, and the soft phase is co Co-rich solid solution. For the alloy with Nb and W, these elements are segregated in the Co-rich solution and for this reason the minimum values of the microhardness are higher for this alloy compared with the alloys without Nb and W. The heat treatment has been chosen to homogenize the alloy's



**Figure 4. SEM micrographs and EDX spectra for S1 (a, b), S2 (c, d) and S3 (e, f) before heat treatment.**

microstructure and it was found that facilitate the precipitation of the carbide phase from the eutectic. Therefore, the value of the maximum hardness increases for each heat-treated sample compared to untreated sample.

### Electrochemical Tests

Following a 24-hour testing period, the corrosion potential versus time curves were examined (refer to Figure 8a) and Table 3. Under these circumstances, the potential—known as the open-circuit potential or OCP—indicates the sample's propensity to resist corrosion. According to the data acquired, the curves of the three untreated samples (S1, S2 and S3) exhibit comparable behavior with a rapid increase in potential, reaching values between  $-0.28$  V and  $-0.26$  V following the first two hours of immersion. This is because the dental materials have been passivated. Therefore, the passive layer of all three alloys remained

unharmful after 2 h of immersion. Then, after 12 h of immersion, the corrosion potential of S1 remains the same, S2 tends to increase and, for S3, it tends to decrease slightly. In general, during the 24-h test, the potential of S1 and S2 samples increased and S3 remained the same due to thickening of the passive film, reaching final values from  $-0.22$  V to  $-0.28$  V.

In the case of the potential curves of the water-cooled samples, during the first 2 h of immersion, they tended to grow, while at 12 hours, it can be seen that S1W grows, S2W decreases slightly and S3W remains constant. This phenomenon is maintained at the end of the test, reaching values between  $-0.03$  and  $-0.30$  V.

The curves of the corrosion potentials of the samples cooled in the oven (S1Ov, S2Ov and S3Ov) show in the first 2 h of the test the movement of these potentials toward less negative values. After 12 h, the potentials of S1Ov and

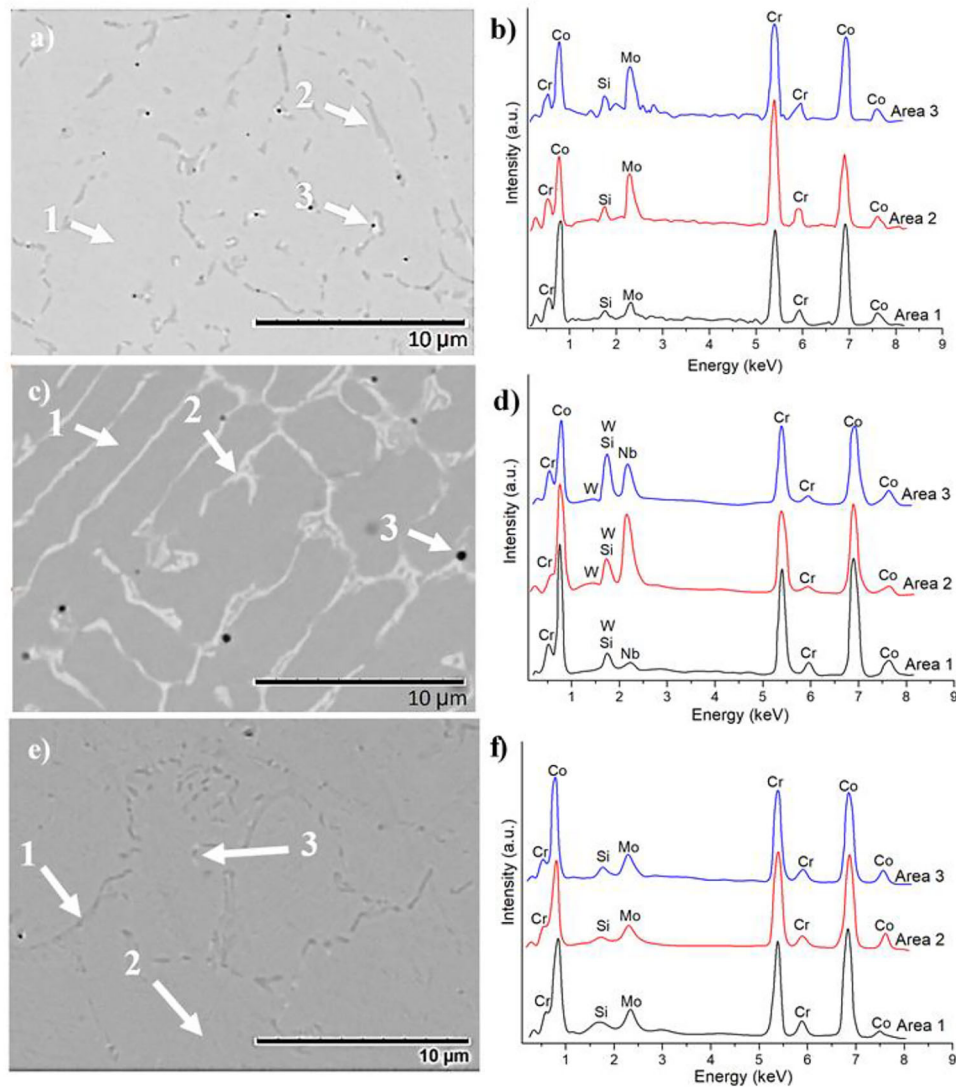


**Figure 5.** SEM micrographs and EDX spectra for S10v (a, b), S20v (c, d) and S30v (e, f).

S30v continue to increase, while for S20v, the potential decreases. After 24 h of testing, it is observed that S10v and S30v remain stable and S20v decreases slightly.

Thus, in general, all nine samples have shown adequate behavior with a tendency to passivation when immersed in Ringer's solution, with smooth potential changes, except S2W and S20v, which had a slight tendency to corrosion.

Likewise, S3W showed high stability, as did S10v and S30v, during the 24-h test. Open-circuit potential analysis indicated passive behavior in all the samples with the best stability at the high potential of S1W due to the higher Cr content and the formation of a protective  $\text{Cr}_2\text{O}_3$  passive layer.

On a semi-logarithmic scale of the present results, Figure 8b displays the findings of the linear polarization

technique, which was used to measure the alloys' rate of corrosion.

Table 4 displays the anodic corrosion potential ( $E_{\text{CORR}}$ ) and corrosion current ( $I_{\text{CORR}}$ ) values, which represent the degree of oxidation of the alloy. Plotting the curve against the open-circuit potential (OCP) across a range of 0.25 V allowed for the determination of the Tafel slopes ( $\beta_c$  and  $\beta_a$ ). An alloy with a higher probability of passivation will have  $\beta_a$  greater than  $\beta_c$ . In this case, the surface of all nine samples exhibited a tendency to passivate and create a protective passive layer.

Additionally, Table 4 displays the Tafel curve parameters and the corrosion rate (CR) of the tested samples using the corrosion current, the equivalent weight (EW) in g/eq, the density ( $d$ ) in  $\text{g}/\text{cm}^3$ , the area ( $A$ ) of each sample (in  $\text{cm}^2$ ) and the constant ( $K$ ) that establishes the corrosion rate units ( $1.288 \cdot 10^5$  miliinches/A-cm-year).

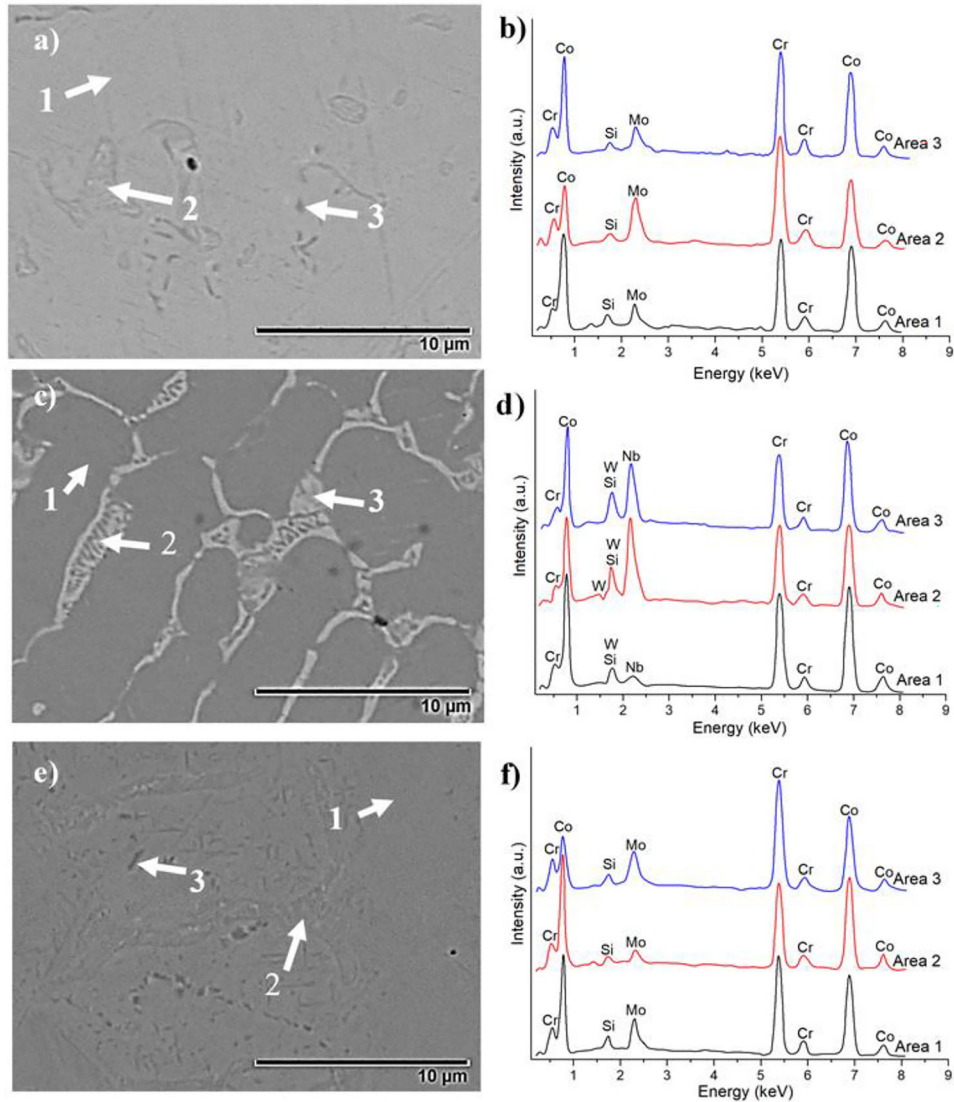


**Figure 6. SEM micrographs and EDX spectra for S1W (a, b), S2W (c, d) and S3W (e, f).**

$$CR = \frac{I_{corr} \cdot K \cdot EW}{d \cdot A} \quad \text{Eqn. 1}$$

A minimum CR of  $1.01 \cdot 10^{-3}$  mpy (S2Ov) and a maximum CR of  $8.86 \cdot 10^{-3}$  mpy (S1) were achieved. When analyzing the samples with the same composition, it is predicted that, when heat treatment is applied, the CR decreases, while for the S3 group, the CR increases. A higher corrosion rate value of  $3.27 \cdot 10^{-3}$  mpy was obtained for S2W, which has the same composition as S2.

Figures 9 and 10 show the Nyquist and Bode impedance and phase diagrams, respectively, obtained at open-circuit potential.

Analyzing the Nyquist plot in Figure 9, it is demonstrated that the higher the values of the real impedance and the

imaginary impedance, the higher the corrosion resistance and the more capacitive the behavior of the samples. This means that the more capacitive the samples behave, the larger the arcs are plotted. In this regard, the heat-treated and water-cooled samples, such as S2W, stand out with the highest real impedance ( $Z' \approx 1.11 \cdot 10^5 \text{ Ohm} \cdot \text{cm}^2$ ) and significant imaginary impedance ( $Z'' \approx 1.20 \cdot 10^5 \text{ Ohm} \cdot \text{cm}^2$ ), suggesting excellent corrosion resistance and superior capacitive behavior. On the other hand, samples S1Ov, S1, S2 and S3 present lower real impedances, indicating a higher susceptibility to corrosion, while the imaginary impedance values are quite high and thus present a capacitive arc. In the case of S1W, both the real impedance ( $Z' \approx 4.10 \cdot 10^4 \text{ Ohm} \cdot \text{cm}^2$ ) and the imaginary impedance ( $Z'' \approx 5.33 \cdot 10^4 \text{ Ohm} \cdot \text{cm}^2$ ) are the lowest, indicating a lower polarization capacity and thus a less favorable corrosion resistance. This behavior underlines the importance of heat treatment and water quenching,

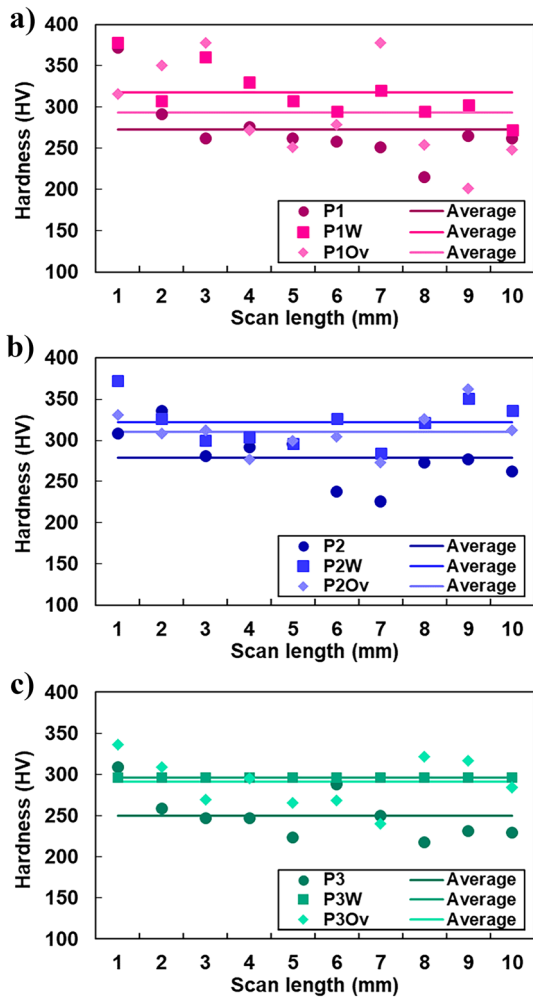


Figure 7. Microhardness values for each indentation for: (a) S1, S1W and S1Ov, (b) S2, S2W and S2Ov and (c) S3, S3W and S3Ov, under loadings of 10 gf.

Table 2. Microhardness Values of the Nine Samples After Applying 10 gf

Sample	Microhardness (HV)				Depth( $\mu$ m)
	Average	Deviation	Maximum	Minimum	
S1	272	40	373	216	1.67
S1W	318	32	378	273	1.54
S1Ov	294	60	379	202	1.60
S2	279	32	336	226	1.65
S2W	322	27	373	284	1.53
S2Ov	311	26	362	273	1.56
S3	250	29	309	218	1.74
S3W	296	25	331	259	1.60
S3Ov	291	41	336	266	1.61

which appear to significantly improve corrosion resistance compared to untreated or less effectively treated samples.

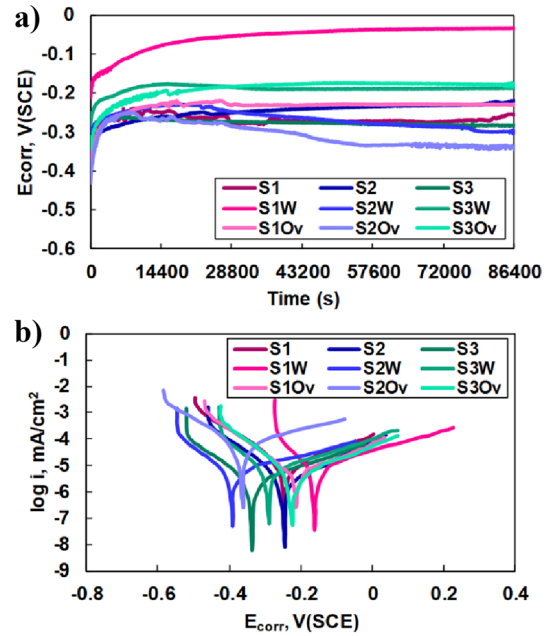


Figure 8. (a) Open-circuit potential after 24 h immersion time; (b) linear polarization curves.

Table 3. Corrosion Potential Results: Initial, After 2 Hours, After 12 Hours and 24 Hours of Immersion of the Samples in Ringer Grifols Electrolyte

Sample	Potential (V)			
	Initial	After 2 h	After 12 h	After 24 h
S1	-0.33	-0.27	-0.27	-0.25
S1W	-0.21	-0.11	-0.04	-0.03
S1Ov	-0.40	-0.25	-0.23	-0.23
S2	-0.35	-0.28	-0.24	-0.22
S2W	-0.30	-0.25	-0.26	-0.30
S2Ov	-0.43	-0.25	-0.31	-0.34
S3	-0.28	-0.26	-0.28	-0.28
S3W	-0.28	-0.19	-0.19	-0.19
S3Ov	-0.34	-0.22	-0.18	-0.18

The Bode plot in Figure 10a shows the relationship between frequency and impedance magnitude ( $|Z|$ ) and the results obtained are shown in Table 4. The samples S2W, S2, S1 and S3W reach very high and similar impedance values, in the order of  $1.60 \cdot 10^5$  Ohm $\cdot$ cm $^2$  at a frequency of 0.1 Hz, indicating excellent corrosion resistance at low frequency conditions. This behavior suggests that these samples are effective in resisting corrosive processes, especially at low frequencies where corrosion is more likely to occur. On the other hand, sample S1W shows the lowest impedance value, followed by S2Ov, indicating lower corrosion resistance and suggesting that, in this case, the heat treatment and cooling conditions do not confirm an

**Table 4. Corrosion Parameters for all Samples Tested**

Sample	E <sub>corr</sub> (V)	I <sub>corr</sub> (μA)	β <sub>a</sub> (mV)	β <sub>c</sub> (mV)	CR (mpy)
S1	-237.56	0.013	235.00	129.60	8.86·10 <sup>-3</sup>
S1W	-219.30	0.006	266.10	29.80	3.57·10 <sup>-3</sup>
S1Ov	-210.47	0.006	207.60	118.50	4.09·10 <sup>-3</sup>
S2	-237.98	0.003	170.90	109.50	1.65·10 <sup>-3</sup>
S2W	-425.78	0.006	381.60	75.10	3.27·10 <sup>-3</sup>
S2Ov	-368.69	0.069	311.60	134.10	1.01·10 <sup>-3</sup>
S3	-346.91	0.003	252.00	101.30	2.01·10 <sup>-3</sup>
S3W	-319.39	0.005	259.9	64.20	3.19·10 <sup>-3</sup>
S3Ov	-227.38	0.005	216.30	93.70	3.50·10 <sup>-3</sup>

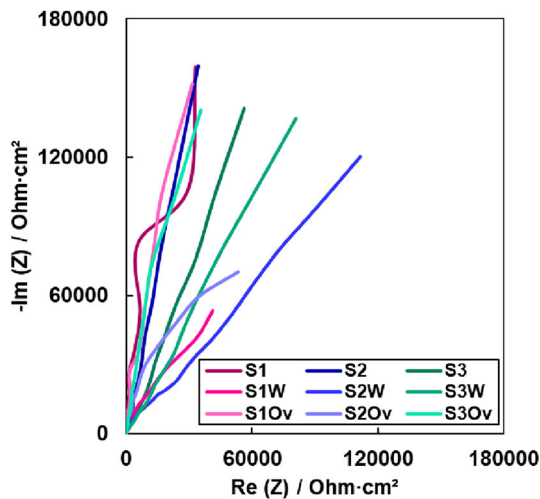


**Figure 9. Nyquist diagrams at 0.00 V versus OCP of the studied samples.**

improvement in the corrosion protection of the materials analyzed.

Analyzing the Bode phase diagram in Figure 10b and the results obtained in Table 5, a large variation in phase angles between 0.1 and 1 Hz is observed, reflecting different electrochemical behaviors among the samples. Samples S2W, S3 and S3W reach their maximum angles around 1000 Hz, indicating more capacitive behavior at high frequencies. However, as the frequency decreases toward 0.1 Hz, the phase angles of these samples decrease considerably, the reduction being most pronounced in sample S2, which reaches approximately  $-47^\circ$ . This drop in phase angles at low frequencies suggests a lower charge storage capacity, which could be related to a decrease in corrosion resistance under these conditions. On the other hand, samples that maintain higher phase angles over a wide range of frequencies, such as S1Ov and S1, show better capacitive behavior, which translates into higher corrosion resistance. In summary, the phase as a function of frequency provides key information about the

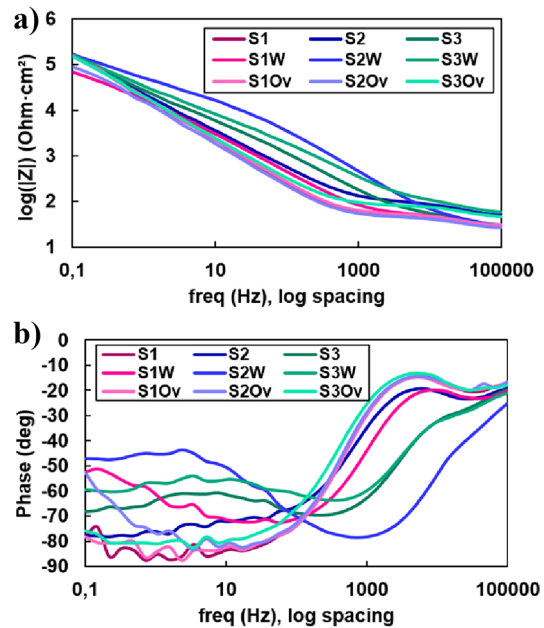


**Figure 10. Bode-|Z| and Bode phase diagrams at 0.00 V versus OCP of the studied samples.**

**Table 5. Results from the Samples' Bode Diagrams Under Study at 0.00 V Versus OCP**

Sample	Bode impedance (Ohm·cm <sup>2</sup> )	Bode phase (°)
S1	1.62·10 <sup>5</sup>	87.62
S1W	6.73·10 <sup>4</sup>	72.35
S1Ov	1.55·10 <sup>5</sup>	87.60
S2	1.63·10 <sup>5</sup>	78.33
S2W	1.64·10 <sup>5</sup>	78.49
S2Ov	8.81·10 <sup>4</sup>	83.47
S3	1.52·10 <sup>5</sup>	69.64
S3W	1.59·10 <sup>5</sup>	63.50
S3Ov	1.45·10 <sup>5</sup>	82.61

electrochemical stability of the samples and their ability to protect against corrosion.

By adding a capacitive component to the impedance, a persistent, well-formed passive layer on the surface of a sample raises the phase angle and modifies the phase response. As shown in Figure 11, a computational model based on the equivalent electrical circuit (EEC) was used to simulate the impedance spectra in order to gain a better understanding of the properties of the corrosion layer structure. The ZSimpWin software fitting yielded the following primary parameters: 1) The solution resistance is denoted by R<sub>sol</sub>; 2) the porous and 3) the compact passive layers are represented by the two parallel pairs R<sub>1</sub>/CPE<sub>1</sub> and R<sub>2</sub>/CPE<sub>2</sub>, respectively. Due to the heterogeneous nature of the passive film in alloys, the non-ideal capacitive

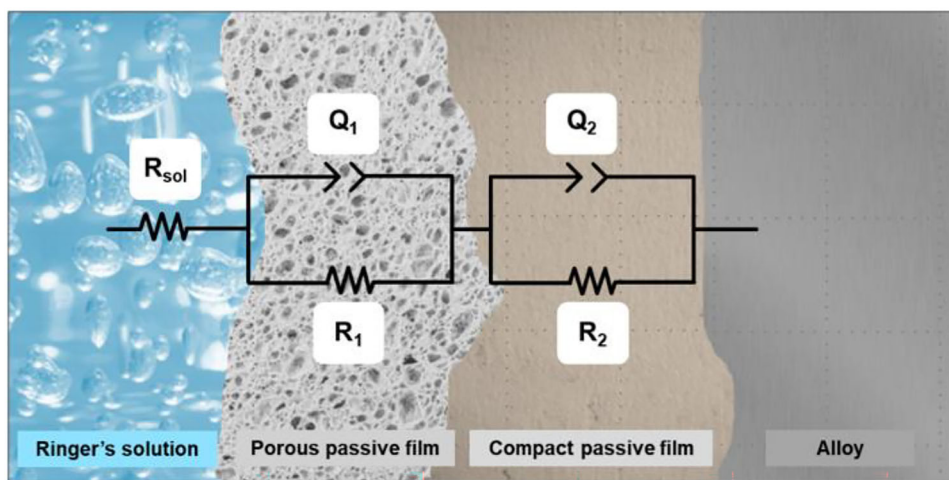


Figure 11. Equivalent circuit  $R(QR)(QR)$ .

Table 6. Equivalent Electric Circuit ( $R(QR)(QR)$ ) Parameters for Fitting the Electrochemical Impedance Spectroscopy Data

Samples	$Y_1$ (S·sec <sup>n</sup> /cm <sup>2</sup> )	$n_1$	$R_1$ (Ohm·cm <sup>2</sup> )	$Y_2$ (S·sec <sup>n</sup> /cm <sup>2</sup> )	$n_2$	$R_2$ (Ohm·cm <sup>2</sup> )
S1	$8.30 \cdot 10^{-6}$	0.74	16.38	$1.79 \cdot 10^{-5}$	0.95	$5.00 \cdot 10^5$
S1W	$6.14 \cdot 10^{-7}$	0.95	13.19	$2.07 \cdot 10^{-5}$	0.82	$6.12 \cdot 10^4$
S1Ov	$1.79 \cdot 10^{-5}$	0.94	16.32	$8.30 \cdot 10^{-6}$	0.75	$5.70 \cdot 10^5$
S2	$6.46 \cdot 10^{-7}$	0.87	52.03	$9.30 \cdot 10^{-6}$	0.83	$5.12 \cdot 10^6$
S2W	$1.90 \cdot 10^{-6}$	0.91	$1.05 \cdot 10^4$	$9.36 \cdot 10^{-6}$	0.79	$1.88 \cdot 10^5$
S2Ov	$4.67 \cdot 10^{-6}$	0.79	16.02	$1.95 \cdot 10^{-5}$	0.93	$9.58 \cdot 10^4$
S3	$1.69 \cdot 10^{-5}$	0.90	$5.46 \cdot 10^3$	$2.17 \cdot 10^{-5}$	0.74	$3.42 \cdot 10^5$
S3W	$7.59 \cdot 10^{-6}$	1.00	$8.84 \cdot 10^2$	$1.57 \cdot 10^{-5}$	0.68	$6.28 \cdot 10^6$
S3Ov	$1.92 \cdot 10^{-5}$	0.91	26.47	$5.35 \cdot 10^{-6}$	0.73	$9.29 \cdot 10^5$

response is emphasized by substituting with a constant phase element (CPE) the pure capacitance. The following equation may be used to calculate the CPE's electrical impedance<sup>35</sup>:

$$Z_{CPE} = Y^{-1}(j\omega)^{-n} \quad \text{Eqn. 2}$$

where  $Y$  is a constant with dimensions of  $\Omega^{-1} \cdot s^n$  (also called the CPE coefficient or pseudo-capacitance),  $j$  is the imaginary unit ( $j^2 = -1$ ),  $\omega$  is the angular frequency and  $n$  is the CPE exponent (with  $0 \leq n < 1$ ). The CPE acts like a perfect capacitor when  $n = 1$  and like a pure resistor when  $n = 0$ .

The parameters extracted from the fitting of experimental data are listed in Table 6. The heat treatment and cooling method have a significant impact on the equivalent circuit parameters  $R(QR)(QR)$  and thus on the corrosion resistance of the samples. However, no clear and consistent improvement in corrosion resistance is observed for the

heat-treated samples. Samples S3W and S2 have the highest total resistance values ( $R_1 + R_2$ ) with values around  $10^6$  Ohm·cm<sup>2</sup>, suggesting higher corrosion resistance, while samples S1W and S2Ov have the lowest total resistance values of  $10^4$  Ohm·cm<sup>2</sup>, indicating lower corrosion resistance. In addition, the values of ( $Y_1$ ) and ( $Y_2$ ) and their respective exponents ( $n_1$ ) and ( $n_2$ ) also show significant variations, suggesting differences in charge storage capacity and relaxation time distribution. Furthermore, the applied equivalent circuit matched very well the results measured with a  $\chi^2$  of about  $10^{-4}$ . In summary, although the heat treatment and cooling method influence the electrochemical parameters, they cannot be analyzed generically but grouped by composition. In this case, sample S1 is not particularly improved by heat treatment, S2 shows a higher corrosion resistance and S3 does improve in corrosion resistance when heat treated and water quenched (S3W). Other factors, such as the specific

microstructure of each sample or the homogeneity of the heat treatment, could influence the results.

It can be observed that the sample with Nb and W and water quenched has a high resistance of the exterior layer of the passive film due to the absence of the pores in the microstructure. Although water quenching introduces residual stress, these can act as a barrier to the propagation of active corrosion centers. In addition, during furnace quenching, alloys remain at elevated temperatures for longer periods of time, which facilitates the formation of oxides and porous, inhomogeneous surface layers. So, there are certain zones that are more susceptible to corrosion and therefore, the alloys have less resistance to the corrosion process.

## Conclusions

Based on the results discussed in this work, after analyzing the three dental alloys and the effect of heat treatment on them, the following conclusions are presented:

- The casting samples S1 and S3 present pores in comparison with sample S2. This is because the sample S2 contains Nb and W with high melting points so, the casting process is done at higher temperature, which improves sample homogeneity and eliminates pores. The samples cooled in the oven show a coarsening in dendrites while those cooled in the water show finer dendrites.
- The microhardness was higher in the heat-treated samples compared with casting samples, suggesting an increase in resistance to localized indentation-induced deformation.
- The heat-treated samples showed remarkable stability and high corrosion resistance. Open-circuit potential analysis indicated passive behavior in all the samples with the best stability at the high potential of S1W due to the higher Cr content and the formation of a protective  $\text{Cr}_2\text{O}_3$  passive layer.
- Electrochemical impedance results confirmed that water-quenched samples exhibited high impedance values due to the residual stress that can prevent active corrosion centers from developing. During furnace quenching, alloys remain at high temperatures longer, generating oxides and porous, inhomogeneous surface layers. Certain zones are more sensitive to corrosion; hence, alloys are less corrosion resistant.

## Acknowledgements

This paper is an invited submission to IJMC selected from presentations at the 3rd Carl R. Loper Conference on Processing of Metallic Materials through Casting

and Solidification held September 23-25,2024, at the Sergiu T. Chiriacescu Aula of Transilvania University, Brasov, Romania. We hereby acknowledge the European project 2023-1-RO01-KA220-HED-000159985: Smart Healthcare Engineering.

**Author contributions** Conceptualization: Cristina Jiménez-Marcos; Methodology: Julia Claudia Mirza-Rosca; Formal analysis and investigation: Cristina Jiménez-Marcos, Dinu Vermesan; Writing—original draft preparation: Cristina Jiménez-Marcos, Dinu Vermesan; Writing—review and editing: Julia Claudia Mirza-Rosca; Funding acquisition: Julia Claudia Mirza-Rosca; Supervision: Adriana Saceleanu.

## Funding

Open Access funding provided thanks to the CRUE-CSIC agreement with Springer Nature.

**Conflict of interest** The authors do not have any conflicts of interest in relation to this article. The authors have no financial or proprietary interests in any material discussed in this article.

**Open Access** This article is licensed under a Creative Commons Attribution 4.0 International License, which permits use, sharing, adaptation, distribution and reproduction in any medium or format, as long as you give appropriate credit to the original author(s) and the source, provide a link to the Creative Commons licence, and indicate if changes were made. The images or other third party material in this article are included in the article's Creative Commons licence, unless indicated otherwise in a credit line to the material. If material is not included in the article's Creative Commons licence and your intended use is not permitted by statutory regulation or exceeds the permitted use, you will need to obtain permission directly from the copyright holder. To view a copy of this licence, visit <http://creativecommons.org/licenses/by/4.0/>.

## REFERENCES

1. C.D. Lynch, V.R. O'Sullivan, C.T. McGillicuddy, Pierre Fauchard: the 'Father of Modern Dentistry.' *Br. Dent. J.* **201**, 779–781 (2006). <https://doi.org/10.1038/sj.bdj.4814350>
2. G.L. Turdean, A. Craciun, D. Popa, M. Constantiniuc, Study of electrochemical corrosion of biocompatible Co–Cr and Ni–Cr dental alloys in artificial saliva. Influence of pH of the solution. *Mater. Chem. Phys.* **233**, 390–398 (2019). <https://doi.org/10.1016/j.matchemphys.2019.05.041>
3. C.M. Garcia-Falcon, T. Gil-Lopez, A. Verdu-Vazquez, J.C. Mirza-Rosca, Analysis and comparison of the corrosive behavior of nickel-based and cobalt-based dental alloys. *Materials* **14**(17), 4949 (2021). <https://doi.org/10.3390/MA14174949>
4. G. Alp, G. Çakmak, M. Sert, Y. Burgaz, Corrosion potential in artificial saliva and possible genotoxic and cytotoxic damage in buccal epithelial cells of patients who underwent Ni-Cr based porcelain-fused-to-metal fixed dental prostheses. *Mutat. Res. Toxicol. Environ. Mutagen.* **827**, 19–26 (2018). <https://doi.org/10.1016/J.MRGENTOX.2018.01.004>

5. V. Torabinejad, M. Aliofkhaezraei, S. Assareh, M.H. Allahyarzadeh, A.S. Rouhaghdam, Electrodeposition of Ni-Fe alloys, composites, and nano coatings—A review. *J. Alloys Compd.* **691**, 841–859 (2017). <https://doi.org/10.1016/J.JALLCOM.2016.08.329>
6. C.M. Garcia-Falcon, T. Gil-Lopez, A. Verdu-Vazquez, J.C. Mirza-Rosca, Corrosion behavior in Ringer solution of several commercially used metal alloys. *Anti-Corrosion Methods Mater.* **68**, 324–330 (2021). <https://doi.org/10.1108/ACMM-05-2021-2486>
7. P. Liliana, S.C. Elena, C.L. Virgil, D.M. Laurentiu, P.S. Daniel, Corrosion behavior of Ni-Cr dental casting alloys. *Int. J. Electrochem. Sci.* **13**, 410–423 (2018). <https://doi.org/10.20964/2018.01.08>
8. L. Gerhardtsson, Diagnosis and treatment of metal poisoning general aspects, in *Handbook on the Toxicology of Metals*. (Elsevier, 2022), pp.663–684. <https://doi.org/10.1016/B978-0-12-823292-7.00017-6>
9. Y. Lu, W. Chen, W. Ke, S. Wu, Nickel-based (Ni–Cr and Ni–Cr–Be) alloys used in dental restorations may be a potential cause for immune-mediated hypersensitivity. *Med. Hypotheses* **73**, 716–717 (2009). <https://doi.org/10.1016/J.MEHY.2009.04.041>
10. L. Reclaru et al., Ni–Cr based dental alloys; Ni release, corrosion and biological evaluation. *Mater. Sci. Eng. C* **32**, 1452–1460 (2012). <https://doi.org/10.1016/J.MSEC.2012.04.025>
11. C.M. Garcia-Falcon, T. Gil-Lopez, A. Verdu-Vazquez, J.C. Mirza-Rosca, Electrochemical characterization of some cobalt base alloys in Ringer solution. *Mater. Chem. Phys.* **260**, 124164 (2021). <https://doi.org/10.1016/J.MATCHEMPHYS.2020.124164>
12. S. Mercieca, M. Caligari Conti, J. Buhagiar, J. Camilleri, Assessment of corrosion resistance of cast cobalt- and nickel-chromium dental alloys in acidic environments. *J. Appl. Biomater. Funct. Mater.* **16**, 47–54 (2018). <https://doi.org/10.5301/jabfm.5000383>
13. Y.S. Al Jabbari, Physico-mechanical properties and prosthodontic applications of Co-Cr dental alloys: a review of the literature. *J. Adv. Prosthodont.* **6**, 138–145 (2014). <https://doi.org/10.4047/JAP.2014.6.2.138>
14. B. Grosogeat, A. Vaicelyte, R. Gauthier, C. Janssen, M. Le Borgne, Toxicological risks of the cobalt-chromium alloys in dentistry: a systematic review. *Materials (Basel)* (2022). <https://doi.org/10.3390/MA15175801>
15. M.C. Conti, A. Karl, P.S. Wismayer, J. Buhagiar, Biocompatibility and characterization of a Kolsterised® medical grade cobalt-chromium-molybdenum alloy. *Biomater* **4**, e27713 (2014). <https://doi.org/10.4161/biom.27713>
16. E. Kretz, P. Berthod, T. Schweitzer, Corrosion behavior in a neutral artificial saliva of several binary Co-Cr alloys with various chromium contents. *J. Dent. Craniofacial Res.* (2018). <https://doi.org/10.21767/2576-392X.100021>
17. A.L. Ramírez-Ledesma, P. Roncagliolo, M.A. Álvarez-Pérez, H.F. Lopez, J.A. Juárez-Islas, Corrosion assessment of an implantable dental Co-Cr alloy in artificial saliva and biocompatibility behavior. *J. Mater. Eng. Perform.* **29**, 1657–1670 (2020). <https://doi.org/10.1007/s11665-020-04711-2>
18. A. Aherwar, A. Patnaik, M. Bahraminasab, Effect of molybdenum content on structure and properties of a Co-Cr biomedical alloy. *J. Mater. Eng. Perform.* **28**, 6340–6353 (2019). <https://doi.org/10.1007/s11665-019-04356-w>
19. W.A. Uriciuc et al., Study on the surface of cobalt-chromium dental alloys and their behavior in oral cavity as cast materials. *Materials (Basel)* (2022). <https://doi.org/10.3390/MA15093052/S1>
20. R.M. Carranza, M.A. Rodríguez, Crevice corrosion of nickel-based alloys considered as engineering barriers of geological repositories. *npj Mater. Degrad.* **11**(1), 1–9 (2017). <https://doi.org/10.1038/s41529-017-0010-5>
21. A. Vaicelyte, C. Janssen, M. Le Borgne, B. Grosogeat, Cobalt-chromium dental alloys: metal exposures, toxicological risks, CMR classification, and EU regulatory framework. *Crystals* **10**, 1151 (2020). <https://doi.org/10.3390/cryst10121151>
22. P. Sahoo, S.K. Das, J. Paulo Davim, Tribology of materials for biomedical applications, in *Mechanical Behaviour of Biomaterials*. (Elsevier, 2019), pp.1–45. <https://doi.org/10.1016/B978-0-08-102174-3.00001-2>
23. K. Lutton Cwalina, C.R. Demarest, A.Y. Gerard, J.R. Scully, Revisiting the effects of molybdenum and tungsten alloying on corrosion behavior of nickel-chromium alloys in aqueous corrosion. *Curr. Opin. Solid State Mater. Sci.* **23**, 129–141 (2019). <https://doi.org/10.1016/J.COSSMS.2019.03.002>
24. T. Matković, P. Matković, J. Malina, Effects of Ni and Mo on the microstructure and some other properties of Co–Cr dental alloys. *J. Alloys Compd.* **366**, 293–297 (2004). <https://doi.org/10.1016/j.jallcom.2003.07.004>
25. M. Samii Zafarghandi, S.M. Abbasi, A. Momeni, Effects of Nb on hot tensile deformation behavior of cast Haynes 25 Co-Cr-W-Ni alloy. *J. Alloys Compd.* **774**, 18–29 (2019). <https://doi.org/10.1016/j.jallcom.2018.09.301>
26. M.O. Dada, J.O. Abe, A.P.I. Popoola, T.M. Phasani, Effects of Nb and Mo Alloying Elements on the Corrosion Characteristics of Sintered Cobalt-Chromium Alloys in Hanks Solution for Biomedical Application. *J. Bio-Tribo-Corrosion* (2024). <https://doi.org/10.1007/s40735-024-00892-8>
27. A. Ramirez-Ledesma, H. Lopez, J. Juarez-Islas, Evaluation of Chill Cast Co-Cr alloys for biomedical applications. *Metals (Basel)*. **6**, 188 (2016). <https://doi.org/10.3390/met6080188>
28. Y. Zhou et al., Microstructure evolution and mechanical properties improvement of selective laser melted Co-Cr biomedical alloys during subsequent

- heat treatments. *J. Alloys Compd.* **840**, 155664 (2020). <https://doi.org/10.1016/j.jallcom.2020.155664>
29. D.J. da Silva, R. Contieri, A. Cremasco, R. Floriano, The effect of cooling rate on the microstructure and hardness of as-cast Co-28Cr-6Mo alloy used as biomedical knee implant. *Int. J. Met.* **16**, 2187–2198 (2022). <https://doi.org/10.1007/s40962-021-00749-7>
30. A. Saceleanu, N. Florido-Suarez, C. Jimenez-Marco, J. Mirza-Rosca, Relation between composition, structure and properties of different dental alloys. *Microsc. Microanal.* **28**, 684–688 (2022). <https://doi.org/10.1017/S1431927622003221>
31. A. I. W. Conshohocken. ASTM E3-11(2017); Standard Guide for Preparation of Metallographic Specimens. (2017).
32. International Organization for Standardization. ISO 14577-1:2015 Metallic materials — Instrumented indentation... (2015).
33. ISO 10271:2020 - Dentistry — Corrosion test methods for metallic materials. (2020).
34. ISO 16773-1-4:2016 Electrochemical impedance spectroscopy (EIS) on coated and uncoated metallic specimens. (2016).
35. B.A. Boukamp, A Nonlinear Least Squares Fit procedure for analysis of immittance data of electrochemical systems. *Solid State Ionics* **20**, 31–44 (1986). [https://doi.org/10.1016/0167-2738\(86\)90031-7](https://doi.org/10.1016/0167-2738(86)90031-7)

**Publisher's Note** Springer Nature remains neutral with regard to jurisdictional claims in published maps and institutional affiliations.